

See discussions, stats, and author profiles for this publication at: <https://www.researchgate.net/publication/269631776>

# Discerning Site Selectivity on Graphene Nanoflakes Using Conceptual Density Functional Theory Based Reactivity Descriptors

ARTICLE in THE JOURNAL OF PHYSICAL CHEMISTRY C · OCTOBER 2014

Impact Factor: 4.77 · DOI: 10.1021/jp505634q

---

CITATIONS

2

---

READS

203

## 3 AUTHORS:



Nazrulla Mohammed Azeezulla

Central Electrochemical Research Institute

4 PUBLICATIONS 2 CITATIONS

[SEE PROFILE](#)



Sailaja Krishnamurty

Central Electrochemical Research Institute

54 PUBLICATIONS 893 CITATIONS

[SEE PROFILE](#)



Kanala Phani

Central Electrochemical Research Institute

92 PUBLICATIONS 1,773 CITATIONS

[SEE PROFILE](#)

# Discerning Site Selectivity on Graphene Nanoflakes Using Conceptual Density Functional Theory Based Reactivity Descriptors

Mohammed Azeezulla Nazrulla and Sailaja Krishnamurty\*

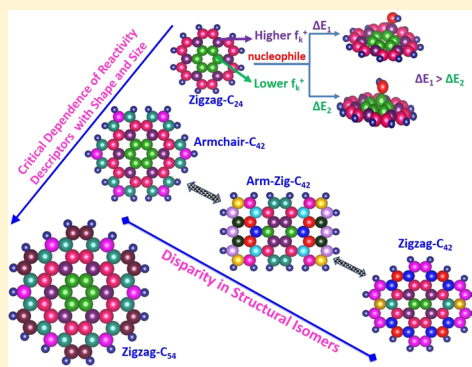
Functional Materials Division, CSIR-Central ElectroChemical Research Institute, Karaikudi 630006, India

K. L. N. Phani

Electrodics and Electro-Catalysis Division, CSIR-Central ElectroChemical Research Institute, Karaikudi 630006, India

## Supporting Information

**ABSTRACT:** Graphene nanoflakes (GNFs) have more configurational degrees of freedom as compared to Graphene nanoribbons (GNRs) and are viable candidates for future nanodevices. GNFs can be devised with disparate geometries, and their electronic properties can be fine-tuned by genuine chemical functionalization. Hence, it is vital to know specific sites on GNFs where reaction is most feasible for chemical functionalization with donor–acceptor functional groups (nucleophiles/electrophiles). Here, we present spin-polarized and dispersion-corrected density functional theory based relative reactivity descriptor calculations to shed light on the reactivity pattern in small-sized GNFs. To have a clear understanding on the structure–property relationship, we consider GNFs with 24, 42, and 54 carbon atoms having various edges, namely, fully armchair, armchair/zigzag (arm-zig), and fully zigzag. All the edge atoms are saturated by hydrogen atoms. On the basis of the symmetry of the GNFs, susceptibility of assorted reactive sites pertinent to nucleophilic and electrophilic attacks is anticipated using relative reactivity descriptors. Further, we validate these relative reactivity descriptors for nucleophilic attack on armchair- $C_{24}H_{14}$  and zigzag- $C_{24}H_{12}$  by explicit adsorption of  $OH^-$ ,  $NH_2^-$ , and  $H_2O$  molecules. Our study reveals that the reactivity pattern varies in small-sized GNFs as a function of shape. Importantly, few specific structural isomers have alternate Lewis acid–base pairs. It also manifests how the reactivity of peripheral and interior carbon atoms differ with shape and size of GNFs. With a discernment on site selectivity, GNFs can be functionalized by proper donor–acceptor groups at specific sites and hence can be used as potential candidates for molecular- and nanoelectronics.



## 1. INTRODUCTION

One of the most exciting advancements in the field of nanoscience and nanotechnology is the synthesis of a multifunctional material, graphene,<sup>1</sup> a two-dimensional (2D) atomically thick layer of graphite with a honeycomb bipartite lattice structure. As a consequence of massless Dirac Fermions,<sup>2</sup> graphene possesses several unique properties such as anomalous room-temperature quantum hall effect,<sup>3</sup> Klein tunneling,<sup>4</sup> extremely high carrier mobility,<sup>5</sup> high thermal/electrical conductivity,<sup>6</sup> good optical transparency,<sup>7</sup> and ambipolar electric field effect.<sup>8</sup> Because of these exceptional properties, graphene is being used in various applications. Despite its wide range of properties, graphene faces severe limitation in the field of nanoelectronics and spintronics, due to vanishingly small density of states at the Fermi level and a zero band gap.<sup>9,10</sup> Owing to the need for rapid growth in discovering novel nanomaterials for meeting increasing energy demands, a plethora of methods have been proposed to overcome this fundamental limitation via either chemical functionalization or size quantization.

Yan et al.<sup>11,12</sup> have shown that electronic properties of graphene can be modified by converting it to an oxide. The most familiar chemically derived form is graphene oxide or reduced graphene oxide<sup>13</sup> consisting of epoxy/hydroxyl groups at the basal plane and carbonyl/carboxyl groups at the edges.<sup>14</sup> In addition to oxidation, a 2D hydrogenation is also seen to convert graphene into a semiconductor with a tunable band gap,<sup>15–17</sup> and partial hydrogenation is seen to incorporate magnetic effects.<sup>18</sup> Band gap can also be tuned by size quantization (miniaturization), that is, by reducing the dimensionality of graphene to nanosize. When cut into nanoribbons,<sup>19,20</sup> graphene (referred to as one-dimensional graphene nanoribbons, 1D GNRs) exhibits a finite band gap that is seen to vary as a function of width, shape, edge structure, and chemical terminations,<sup>9,10</sup> which in turn yields a range of materials such as metals, semiconductors, half metals, ferromagnets, and antiferromagnets. Two major types of finite

Received: June 6, 2014

Revised: September 17, 2014

Published: September 17, 2014



size effects are observed in GNRs, namely, a standing wave state<sup>21,22</sup> and the edge state.<sup>23–25</sup> It is reported that properties such as chemical reactivity, thermodynamic stability, and magnetism in GNRs depend on the type of edges.<sup>26–28</sup> However, there are several limitations in GNRs such as electron mobility degradation and loss of performance in devices.<sup>29,30</sup>

Hence, in addition to 1D GNRs, a zero-dimensional form of graphene, known as graphene nanoflakes (GNFs), alternatively called as polyaromatic hydrocarbons, is produced by both bottom-up<sup>31–33</sup> and top-down approaches.<sup>1,34,35</sup> The virtue of GNFs is that they possess corner states in addition to edge states resulting in a larger number of configurational degrees of freedom as compared to graphene/1D GNRs. Interestingly, it can range in sizes from molecular to semi-infinite 2D structures. As a consequence, its electronic structure is seen to vary from discrete molecular to bandlike with a range of electronic and magnetic properties.<sup>26,27,36</sup> Over the past few years, both experimentally and theoretically, extensive research has been done on GNFs. Shang et al.<sup>37</sup> and Vadukumpully et al.<sup>38–40</sup> have experimentally shown that GNFs can be used in biosensors, energy storage/conversion applications, and conducting composite materials and that chemically functionalized GNFs can be used for catalytic/electronic applications. Theoretically, using density functional theory (DFT)-based methods, it is shown that the stability of GNFs depends on size, shape, space charge,<sup>27,28,41–46</sup> and presence of other chemical groups.<sup>47,48</sup> Several studies have attempted to understand the role of adsorption properties/doping effects/toxicity in tuning the electronic structure of the graphene surface by using simple molecules to metals ions to biomolecules.<sup>49–56</sup> Thermal stability of various sized and shaped GNFs has also been reported.<sup>57,58</sup> More recently, ab initio molecular dynamics (meta-dynamics technique) simulations at high temperatures has revealed a nanoflake-to-cone-to-fullerene transformation.<sup>59</sup>

In spite of extensive research on the geometric and electronic properties of GNFs, very few studies<sup>60,61</sup> address the chemical reactivity of interior and peripheral carbon atoms in GNFs as a function of size and shape. A complete understanding on the reactivity pattern in GNFs is essential for its chemical functionalization toward applications in molecular electronics, organic ferromagnets, and other future nanodevices. In this work, we attempt to propose a means toward predicting the reactivity patterns in GNFs as a function of their size and shape. In order to shed light on the reactivity pattern of interior/peripheral carbon atoms in GNFs and to have a clear understanding on the structure–property relationship, we consider three structural isomers (with respect to carbon atoms) for 24, 42, and 54 carbon atom GNFs with fully armchair, armchair/zigzag (arm-zig), and fully zigzag edges. The arm-zig isomer possesses armchair edges on one side and zigzag on the other side. All the edges of these GNFs are terminated by hydrogen atoms. In our present study, relative reactivity descriptors for GNFs are evaluated using spin-polarized and dispersion-corrected DFT. These relative reactivity descriptors offer substantial insight on the site selectivity for nucleophilic, electrophilic, and radical attacks. In the end, we validate the reactivity trends predicted by relative reactivity descriptors by explicit adsorption of OH<sup>−</sup>, NH<sub>2</sub><sup>−</sup>, and H<sub>2</sub>O on a few reactive sites of two C<sub>24</sub> GNFs.

## 2. THEORETICAL METHODS

On the basis of an idea that electron density  $\rho(\vec{r})$  is a fundamental quantity for describing the atomic and molecular

ground states in DFT,<sup>62</sup> Parr and Yang proposed a tool for deducing the relative reactivity of different sites/positions in a molecule known as Fukui functions,  $f(\vec{r})$ .<sup>63</sup> For a system with  $N$  electrons having the ground state energy  $E[\rho]$  and chemical potential  $\mu$ , a fundamental equation that governs the changes in energy and chemical potential when reactants approach each other is<sup>63</sup>

$$dE = \mu dN + \int \rho(\vec{r}) d\vartheta(\vec{r}) d\vec{r} \quad (1)$$

where  $\vartheta(\vec{r})$  is the external potential at each point  $\vec{r}$  and

$$\mu = \left( \frac{\partial E[\rho(\vec{r})]}{\partial N} \right)_{\vartheta(\vec{r})} \quad (2)$$

Derivative of chemical potential provides a great deal of insight on the chemical reactivity. By differentiating the above equation partially with respect to constant external potential  $\vartheta(\vec{r})$ , we get the response of  $\rho(\vec{r})$  to the number of electrons. Hence, the first derivative of chemical potential with respect to constant external potential or second derivative of energy with respect to number of electrons and external potential defines the Fukui function as

$$f(\vec{r}) \equiv \left[ \frac{\delta \mu}{\delta \vartheta(\vec{r})} \right]_N = \left[ \frac{\partial \rho(\vec{r})}{\partial N} \right]_{\vartheta(\vec{r})} \quad (3)$$

This is the numerical realization of Fukui's frontier molecular orbital theory.<sup>64–66</sup> The derivative involved in calculation of Fukui functions (eq 3) is discontinuous for atoms and molecules.<sup>67–69</sup> So, this  $N$  discontinuity leads to the introduction of both left- and righthand side derivatives for a given number of electrons, and hence, Fukui functions can be calculated by applying the finite difference approximation method. Fukui functions for nucleophilic, electrophilic, and radical attacks can be defined by the finite difference method, using the electron densities of  $N_0$ ,  $(N_0 + 1)$  and  $(N_0 - 1)$  electron systems, respectively as

$$f^+(\vec{r}) \equiv \rho_{N_0+1}(\vec{r}) - \rho_{N_0}(\vec{r}) \quad (4)$$

$$f^-(\vec{r}) \approx \rho_{N_0}(\vec{r}) - \rho_{N_0-1}(\vec{r}) \quad (5)$$

$$f^0(\vec{r}) \approx \frac{1}{2}(\rho_{N_0+1}(\vec{r}) - \rho_{N_0-1}(\vec{r})) \quad (6)$$

where  $\rho_{N_0}(\vec{r})$ ,  $\rho_{N_0+1}(\vec{r})$ , and  $\rho_{N_0-1}(\vec{r})$ , respectively, are the electron densities of  $N_0$ ,  $(N_0 + 1)$ , and  $(N_0 - 1)$  electron systems at a particular point  $\vec{r}$ . The  $f^+(\vec{r})$  and  $f^-(\vec{r})$  are called as local electrophilicity and nucleophilicity indices, respectively.

Parr and Yang<sup>63</sup> pointed out that, in the frozen core approximation,  $f^+(\vec{r})$  and  $f^-(\vec{r})$  can be approximated with density of the lowest unoccupied molecular orbital (LUMO) and the highest occupied molecular orbital (HOMO). Hence,

$$f^+(\vec{r}) \approx \rho^{\text{LUMO}}(\vec{r}) \quad (7)$$

measures the reactivity toward a nucleophilic reagent,

$$f^-(\vec{r}) \approx \rho^{\text{HOMO}}(\vec{r}) \quad (8)$$

measures the reactivity toward an electrophilic reagent, and

$$f^0(\vec{r}) \approx \frac{1}{2}(\rho^{\text{HOMO}}(\vec{r}) + \rho^{\text{LUMO}}(\vec{r})) \quad (9)$$

**Table 1.** Structure, HOMO–LUMO Energy Gap, Dispersion Energy, and Reactivity Descriptors for Hydrogen-Terminated  $C_{24}$  Armchair, Arm-Zig, and Zigzag GNFs<sup>a</sup>

Structure with Bond length(Å)		Sites	$f_k^{el}$	$f_k^{nu}$	Sites	$f_k^{el}$	$f_k^{nu}$	
Armchair $C_{24}H_{14}$		A	0.903	1.113				
		B	1.114	0.914				
		C	0.690	1.379				
		D	0.916	1.092				
		E*	0.171	5.846				
		F*	3.452	0.290				
		G	0.945	1.060				
HOMO-LUMO gap = 2.90 eV								
Dispersion Energy = -10.82 kcalmol <sup>-1</sup>								
Arm-zig $C_{24}H_{14}$		A	0.956	1.045	G	1.020	0.980	
		B	0.981	1.020	H	1.070	0.935	
		C*	0.708	1.415	I	0.994	1.006	
		D	1.007	0.993	J	0.935	1.070	
		E*	1.080	0.925	K	0.984	1.016	
		F	0.962	1.040	L	1.032	0.969	
		HOMO-LUMO gap = 2.11 eV						
Dispersion Energy = -10.71 kcalmol <sup>-1</sup>								
Zigzag $C_{24}H_{12}$		A	1.020	0.980				
		B*	1.052	0.950				
		C*	1.000	1.000				
		HOMO-LUMO gap = 2.86 eV						
Dispersion Energy = -11.54 kcalmol <sup>-1</sup>								

<sup>a</sup>The asterisk (\*) indicates the site with the highest relative reactivity indices, and “ac” indicates armchair pouches. Sites more favorable for a nucleophilic attack are shown in red, and sites more favorable for an electrophilic attack are shown in blue. Sites highlighted in black correspond to amphiphilic sites.

measures the reactivity toward a radical reagent, where  $\rho^{\text{LUMO}}(\vec{r})$  and  $\rho^{\text{HOMO}}(\vec{r})$  are the densities of the LUMO and the HOMO, respectively.

In order to compute the Fukui functions on atomic centers, Yang and Mortier proposed the atom condensed Fukui function,<sup>70</sup> based on an idea of electronic population around

an atom in a molecule, similar to the procedure followed in the population analysis technique. The condensed electrophilicity for an atom  $k$  is defined as

$$f_k^+ \approx q_k^{N_0+1} - q_k^{N_0} \quad (10)$$

Similarly, the condensed nucleophilicity for an atom  $k$  is defined as

$$f_k^- \approx q_k^{N_0} - q_k^{N_0-1} \quad (11)$$

The condensed Fukui function for an atom  $k$  appropriate for the radical attack is defined as

$$f_k^0 \approx \frac{1}{2}(q_k^{N_0+1} - q_k^{N_0-1}) \quad (12)$$

where  $q_k^{N_0}$ ,  $q_k^{N_0+1}$ , and  $q_k^{N_0-1}$  are the electronic populations on an atom  $k$  for the  $N_0$ ,  $(N_0 + 1)$  and  $(N_0 - 1)$  electron systems, respectively.

For comparing site reactivity across the system, a new set of indices are proposed by Roy et al., which are found to be very appropriate for intramolecular reactivity.<sup>71,72</sup> The condensed relative electrophilicity of an atom  $k$  can be defined as

$$f_k^{\text{rel}} \approx \frac{f_k^+}{f_k^-} \quad (13)$$

and the condensed relative nucleophilicity is defined as

$$f_k^{\text{nuc}} \approx \frac{f_k^-}{f_k^+} \quad (14)$$

A site with  $f_k^{\text{rel}} > f_k^{\text{nuc}}$  is more favorable for a nucleophilic attack, while with  $f_k^{\text{nuc}} > f_k^{\text{rel}}$  is clearly a site that is more favorable toward an electrophilic attack. A site for which  $f_k^{\text{rel}}$  is nearly equal to  $f_k^{\text{nuc}}$  is likely to both give or take electrons easily making it an amphiphilic site. Amphiphilic sites are not selective sites and have a small possibility of participating in either oxidation or reduction reactions (with equal possibility). These relative reactivity indices have been very effective in predicting reactivity trends in biomolecules,<sup>73</sup> atomic clusters,<sup>74</sup> nanoparticles,<sup>75</sup> and various other chemically interesting systems.

### 3. COMPUTATIONAL METHODS

In this study, all calculations include spin polarization and are performed within the framework of DFT,<sup>76,77</sup> using linear combinations of Gaussian orbitals as implemented in the deMon.2.2.6 code.<sup>78</sup> The geometries of all hydrogen terminated GNFs are optimized with empirical dispersion<sup>79</sup> effects using the Perdew–Burke–Ernzerhof exchange and correlation functional.<sup>80</sup> The double zeta valence polarization basis set is used for carbon, hydrogen, oxygen, and nitrogen atoms. No additional polarization functions are added. A2 auxiliary functions are added to fit the charge density.<sup>81</sup> The convergence of the geometries is based on the gradient and displacement criteria. Harmonic vibrational frequencies are computed for all the isomers of  $C_{24}$ ,  $C_{42}$ , and  $C_{54}$  GNFs. All frequencies are found to be positive, thereby indicating the optimized isomers of GNFs are local minima.

We have calculated the relative reactivity descriptors for respective optimized geometries of hydrogen-terminated GNFs by the finite difference approximation method on the basis of Löwdin SCF population analysis<sup>82</sup> as discussed in Section 2. Following the reactivity descriptor calculations, for the purpose

of validation, the interaction energy of a GNF with nucleophiles is calculated as

$$E_{\text{AB}}^{\text{int}} = (E_{\text{A}} + E_{\text{B}}) - E_{\text{AB}} \quad (15)$$

where  $E_{\text{A}}$  and  $E_{\text{B}}$  are the energies of GNFs and the nucleophile, respectively.  $E_{\text{AB}}$  is the energy of the GNF–nucleophile complex.

## 4. RESULTS AND DISCUSSION

**4.1. Stability and Site Selectivity in  $C_{24}$  GNFs.** We begin our discussion with three structural isomers (with respect to carbon atoms) of hydrogen-terminated  $C_{24}$  GNFs that are as shown in Table 1. As mentioned in Section 1, the isomers are fully armchair, armchair/zigzag (arm-zig), and fully zigzag edges with hydrogen terminations. Zigzag- $C_{24}\text{H}_{12}$  (coronene) has been extensively used as a model system in many of recent studies,<sup>49,54,58</sup> where its thermal stability, dynamics of ion binding, and adsorption properties are studied. Hence, we have considered the zigzag- $C_{24}\text{H}_{12}$  isomer for our present study. For better understanding of structure–property correlation along with this isomer, we have considered armchair and arm-zig structural counterparts. Among these isomers, the armchair- $C_{24}\text{H}_{14}$  isomer has four armchair pouches (indicated by “ac” in Table 1), and the arm-zig- $C_{24}\text{H}_{14}$  isomer has two armchair pouches (indicated by “ac” in Table 1).

Structure, HOMO–LUMO gap, and dispersion energies of these GNFs are tabulated in Table 1. The HOMO–LUMO gap is known to be an index of both kinetic stability and electrical conductivity. The HOMO–LUMO gaps of  $C_{24}$  armchair, arm-zig, and zigzag GNFs are 2.90, 2.11, and 2.86 eV, respectively. Interestingly, all the atoms in each GNF contribute to both the HOMO and LUMO orbitals (see Supp-Table 1, Supporting Information). However, the directionality of the  $\text{sp}^2$  hybridization varies between each GNF. Dispersion effects/energy play a key role in describing accurate atom-to-atom interactions and its stabilization. Hence, dispersion energy for all structural isomers of  $C_{24}$  GNFs are tabulated in Table 1. The contribution of dispersion energy is between 10–11.5 kcal mol<sup>-1</sup> for all three isomers. The order of dispersion energy contribution toward the total energy of respective isomers is arm-zig < armchair < zigzag.

Silva et al.<sup>57</sup> have reported the out-of-plane-bending mode vibrational frequencies of C–H for zigzag, armchair, and a combination of both zigzag and armchair (in our case, it is designated as arm-zig) GNFs to be 840–941 cm<sup>-1</sup>, 680–840 cm<sup>-1</sup>, and 680–900 cm<sup>-1</sup>, respectively. A similar kind of spectrum is observed for our model systems (see Supp-Figure 1, Supporting Information). In summary, the highest dispersion energy contribution, high HOMO–LUMO energy gap, and a blue shift in C–H (edges) out-of-plane-bending frequencies at the fingerprint region (see Supp-Figure 1, Supporting Information) for the zigzag isomer indicates that zigzag-terminated GNFs are chemically less reactive (more stable) as compared to the rest of the  $C_{24}$  isomers. This observation is corroborated by the fact that zigzag edges are thermally more stable than armchair edges.<sup>57</sup> Site selectivity using relative reactivity descriptors for these GNFs is discussed in following subsections.

**4.1.1. Armchair- $C_{24}\text{H}_{14}$ .** The armchair- $C_{24}\text{H}_{14}$  isomer has seven chemically distinct sites, namely, A–G. Bond length (Å), sites, relative electrophilicity ( $f_k^{\text{rel}}$ ) and nucleophilicity( $f_k^{\text{nuc}}$ ) indices are as shown in Table 1. Among seven chemically

Table 2. Structure, HOMO–LUMO Energy Gap, Dispersion Energy, and Reactivity Descriptors for Hydrogen-Terminated  $C_{42}$  Armchair, Arm-Zig, and Zigzag GNFs<sup>a</sup>

	Structure with Bond length(Å)	Sites	$f_k^{el}$	$f_k^{nu}$	Sites	$f_k^{el}$	$f_k^{nu}$
Armchair $C_{42}H_{18}$	<p>HOMO-LUMO gap = 1.16 eV Dispersion Energy = -22.45 kcalmol<sup>-1</sup></p>	A*	0.960	1.042			
		B	0.985	1.015			
		C*	1.083	0.923			
		D	1.013	0.987			
		E	0.986	1.014			
Arm-zig $C_{42}H_{18}$	<p>HOMO-LUMO gap = 0.27 eV Dispersion Energy = -22.32 kcalmol<sup>-1</sup></p>	A	0.961	1.040	G	0.946	1.057
		B	0.955	1.050	H	1.021	0.980
		C*	1.073	0.932	I	1.000	1.000
		D	1.030	0.971	J	0.964	1.037
		E*	0.903	1.107	K	0.972	1.030
		F	1.014	0.986			
Zigzag $C_{42}H_{16}$	<p>HOMO-LUMO gap = 1.63 eV Dispersion Energy = -23.17 kcalmol<sup>-1</sup></p>	A	0.935	1.069	G	1.019	0.981
		B	1.046	0.956	H	0.976	1.024
		C*	0.931	1.074			
		D*	1.207	0.828			
		E	1.013	0.987			
		F	0.964	1.037			

<sup>a</sup>The asterisk (\*) indicates the sites with the highest relative reactivity indices, and "ac" indicates armchair pouches. Red and blue sites are indicative of sites more favorable for a nucleophilic and an electrophilic attack, respectively. Sites highlighted in black are amphiphilic sites.

different sites, site F has the highest relative electrophilicity index of 3.452 and the lowest relative nucleophilicity index of 0.290 and therefore is the most probable site for attack by nucleophiles. In contrast, site E has the highest index of 5.846 for relative nucleophilicity and the least index of 0.171 for relative electrophilicity and is most susceptible for an attack by electrophiles. Interestingly, sites E and F are adjacent to each other with a bond length of 1.418 Å. Relative reactivity descriptors and bond length for the rest of the sites are as shown in Table 1. Among the rest of the sites, A, C, D, and G have higher  $f_k^{\text{nu}}$  while site B has a higher  $f_k^{\text{el}}$ . Thus, this isomer provides alternate Lewis acid–base pairs with one exceptionally strong catalytically active acid–base pair at armchair pouches. Hence, it is a potential candidate for peripheral functionalization along the armchair pouches and an interesting candidate for functionalization by donor/acceptor functional groups on the surface.

**4.1.2. Arm-Zig- $C_{24}H_{14}$ .** This isomer has zigzag edges on one side and armchair edges on the other as discussed earlier. There are 12 chemically distinct sites in this isomer, namely, A–L (see Table 1). Among the 12 sites, site C has the highest relative nucleophilicity index of 1.415 and the least relative electrophilicity index of 0.708. Site E has the highest relative electrophilicity index of 1.080 and the least relative nucleophilicity index of 0.925. Hence, site C is most susceptible for an electrophilic attack, and site E is most susceptible for a nucleophilic attack. Site C is the interior carbon atom with a C–C bond length of 1.434 Å, and site E is peripheral with an E–E bond length of 1.364 Å. The armchair pouches in this case do not provide strong alternate Lewis acid–base pairs ( $f_k^{\text{el}}$  and  $f_k^{\text{nu}}$  indices are closer to each other in sites G, B, and I). Some of the zigzag edges in this isomer on the other hand have alternate (sites F, H, and J) Lewis acid–base pairs. In short, central atoms are highly reactive as compared to the edge ones, and removing two of the armchair pouches restructures the reactivity pattern (thereby transforming an armchair structure to an arm-zig structure) in armchair- $C_{24}H_{14}$  nanoflake. Lowest dispersion energy contribution, least HOMO–LUMO energy gap, and a red shift in C–H (edges) out-of-plane-bending frequencies at the fingerprint region (see Supp-Figure 1, Supporting Information) with respect to the zigzag isomer are indicative of lower stability of this isomer, which is also projected above by Fukui functions.

**4.1.3. Zigzag- $C_{24}H_{12}$ .** This isomer  $C_{24}H_{12}$  has a nanodisc appearance with only zigzag edges. Owing to the symmetry within this structure, it has only three chemically distinct sites, namely, A–C (see Table 1). Among the three chemically different sites, site B has the highest relative electrophilicity index of 1.052, and therefore, this site is most susceptible for nucleophilic attack. Sites C and A have nearly equal relative nucleophilicity and relative electrophilicity indices. Hence, these sites have an equal probability for an attack by an electrophile/nucleophile and are known as amphiphilic sites. Hence, this structure does not present any strong edge sites for electrophilic or nucleophilic attacks, which implies that edges are nonreactive and the remaining sites are more prone to electrophilic attack. Lesser chemical reactivity of this nanodisc zigzag isomer (coronene) as projected by Fukui functions goes hand in hand with highest dispersion energy contribution, a high HOMO–LUMO gap, and a blue shift in C–H (edges) out-of-plane-bending frequencies at the fingerprint region (see Supp-Figure 1, Supporting Information) for the zigzag isomer.

**4.2. Stability and Site Selectivity in  $C_{42}$  GNFs.** Like zigzag- $C_{24}H_{12}$ , the armchair- $C_{42}H_{18}$  (hexabenzocoronene) isomer has also been extensively studied.<sup>43,57</sup> Hence, we have considered its structural isomers with arm-zig and fully zigzag edges for  $C_{42}$  GNFs along with hexabenzocoronene for better structure–property correlation. The armchair- $C_{42}H_{18}$  isomer has totally six armchair pouches (indicated by “ac” in Table 2), and the arm-zig- $C_{42}H_{18}$  isomer has four armchair pouches (indicated by “ac” in Table 2). Structure, HOMO–LUMO gap, and dispersion energies of  $C_{42}$  GNFs are tabulated in Table 2. The HOMO–LUMO gaps for armchair, arm-zig, and zigzag isomers are 1.16, 0.27, and 1.63 eV, respectively. Also, in this series, each atom contributes to HOMO and LUMO frontier orbitals (see Supp-Table 1, Supporting Information). The trend observed in dispersion energies is similar to those of  $C_{24}$  GNFs, that is, the zigzag isomer has the largest dispersion energy ( $-23.17 \text{ kcal mol}^{-1}$ ), the armchair isomer has a lower dispersion energy of  $-22.45 \text{ kcal mol}^{-1}$ , and the arm-zig isomer has the lowest dispersion energy ( $-22.32 \text{ kcal mol}^{-1}$ ). Also, in this series, the highest dispersion energy contribution, highest HOMO–LUMO energy gap, and a blue shift in C–H (edges) out-of-plane-bending frequencies at the fingerprint region (see Supp-Figure 1, Supporting Information) for the zigzag isomer indicates that the zigzag-terminated GNFs are chemically less reactive (more stable) as compared to the rest of the isomers. Site selectivity using relative reactivity descriptors for these GNFs is discussed in the following subsections.

**4.2.1. Armchair- $C_{42}H_{18}$ .** This nanodisc-shaped isomer is an extension of zigzag- $C_{24}$  with five chemically distinct sites, namely, A–E (see Table 2). Among the five chemically distinct sites, site C has the highest  $f_k^{\text{el}}$  (1.083) and the least relative nucleophilicity value of 0.923. Hence, site C is more susceptible for a nucleophilic attack. Site A has a  $f_k^{\text{nu}}$  value of 1.042 and a  $f_k^{\text{el}}$  value of 0.960 and is most prone to attack by an electrophile. Sites B, D, and E possess nearly the same reactivity indices; hence, these sites are prone to attack by both electrophiles and nucleophiles with the same probability. Thus, this isomer has edges with low reactivity. However, this GNF may be a good candidate for oxidation/reduction reactions on the surface. The presence of sites A and C in close proximity with a spacer B atom makes it highly attractive for simultaneous hydrogenation and dehydrogenation reactions of large molecules.

**4.2.2. Arm-Zig- $C_{42}H_{18}$ .** In this nanomat-shaped isomer, there are 11 chemically distinct sites, namely, A–K (see Table 2). Among the 11 chemically distinct sites, site C has the highest relative electrophilicity value of 1.073 and the least relative nucleophilicity value of 0.932. Therefore, site C is highly susceptible for a nucleophilic attack. Site E has the highest relative nucleophilicity value of 1.107 and the least value for relative electrophilicity of 0.903 and is prone to attack by an electrophile. In addition to these sites, peripheral sites F, H, and I are amphiphilic sites whose  $f_k^{\text{el}}$  and  $f_k^{\text{nu}}$  values are nearly the same. Relative reactivity descriptor indices for this isomer indicate that armchair edges are more prone to attack by nucleophiles, zigzag edges are amphiphilic sites, and the central atoms are very reactive. Hence, the arm-zig- $C_{42}H_{18}$  isomer is a useful candidate for functionalizing more reactive armchair edges with nucleophilic groups and surface functionalization through central reactive sites. Similar to the arm-zig- $C_{24}$  isomer, the arm-zig- $C_{42}$  isomer also has the lowest dispersion energy contribution, least HOMO–LUMO energy gap, and a red shift in C–H (edges) out-of-plane-bending frequencies at the

**Table 3. Structure, HOMO–LUMO Energy Gap, Dispersion Energy, and Reactivity Descriptors for Hydrogen-Terminated  $C_{54}$  Armchair, Arm-Zig, and Zigzag GNFs<sup>a</sup>**

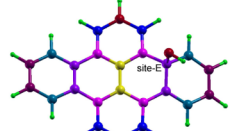
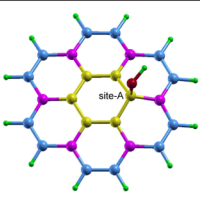
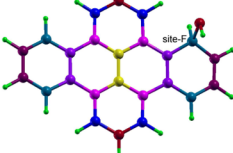
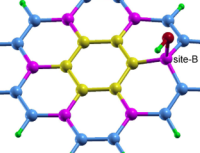
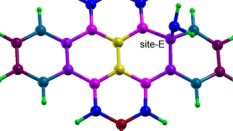
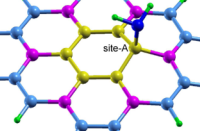
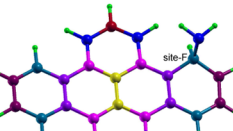
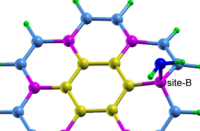
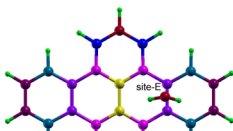
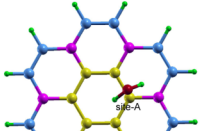
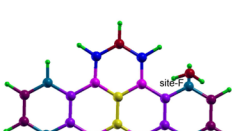
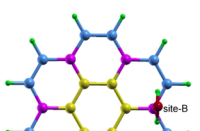
	Structure with Bond length(Å)	Sites	$f_k^{el}$	$f_k^{nu}$	Sites	$f_k^{el}$	$f_k^{nu}$
Armchair $C_{54}H_{22}$	<p>HOMO-LUMO gap = 1.99 eV Dispersion Energy = -29.65 kcalmol<sup>-1</sup></p>	A	0.946	1.057	G	1.008	0.992
		B*	0.870	1.149	H	1.000	1.000
		C	0.965	1.036	I	1.024	0.976
		D*	1.212	0.825	J	1.002	0.998
		E	1.022	0.978	K	1.007	0.993
		F	0.981	1.019			
Arm-zig $C_{54}H_{20}$	<p>HOMO-LUMO gap = 0.02 eV Dispersion Energy = -30.48 kcalmol<sup>-1</sup></p>	A*	1.105	0.905	H	1.007	0.993
		B	0.940	1.064	I	1.035	0.966
		C	0.810	1.234	J	1.021	0.980
		D	0.937	1.067	K	1.047	0.955
		E	0.880	1.136	L	1.027	0.974
		F	1.000	1.000	M	0.914	1.094
		G*	0.771	1.300			
Zigzag $C_{54}H_{18}$	<p>HOMO-LUMO gap = 1.90 eV Dispersion Energy = -31.40 kcalmol<sup>-1</sup></p>	A*	0.983	1.017			
		B*	1.151	0.869			
		C	1.010	0.990			
		D	1.030	0.971			
		E	1.004	0.996			
		F	1.017	0.983			

<sup>a</sup>The asterisk (\*) indicates sites with the highest relative reactivity indices, and "ac" indicates armchair pouches. Sites highlighted in red and blue correspond to sites more prone to nucleophilic and electrophilic attacks, respectively. Sites highlighted in black are not strongly electrophilic or nucleophilic.

fingerprint region (see Supp-Figure 1, Supporting Information) with respect to the zigzag isomer, indicative of lower stability of

this isomer, which goes altogether with reactivity projected by Fukui functions.

Table 4. Adsorption Energies of Various Probe Molecules on Zigzag  $C_{24}H_{12}$  and Armchair  $C_{24}H_{14}$  GNFs<sup>a</sup>

Nucleophile	Armchair geometry	Interaction energy $\text{kcalmol}^{-1}$	Zigzag geometry	Interaction energy $\text{kcalmol}^{-1}$
$\text{OH}^-$		42.71		43.16
				
$\text{NH}_2^-$		51.70		53.53
				
$\text{H}_2\text{O}$		4.45		4.15
				

<sup>a</sup>These energies validate the reactivity trends projected by Fukui functions in Table 1.

**4.2.3. Zigzag- $C_{42}H_{16}$ .** The nanodisc zigzag- $C_{42}H_{16}$  isomer is like a fused dimer of arm-zig- $C_{24}$  with eight chemically different sites, namely, A–H (see Table 2). Among the eight chemically distinct sites, site D has highest relative electrophilicity value of 1.207 and the least index for relative nucleophilicity of 0.828. Hence, this site is more susceptible for an attack by a nucleophile. On the other hand, site C has a  $f_k^{\text{nuc}}$  index of 1.074 and a value of 0.931 for  $f_k^{\text{el}}$ . The sites C and D are bonded with an interatomic distance of 1.430 Å. This isomer thus has Lewis acid–base pairs distributed in the center of the flake while the edges of the flake are less reactive. Alternating Lewis acid–base pairs at the center and the least reactive edges in the isomer makes it a potential candidate for surface functionalization. Similar to the zigzag- $C_{24}$  isomer, lesser chemical reactivity of

this nanodisc zigzag isomer as projected by Fukui functions is in good agreement with the highest dispersion energy contribution, highest HOMO–LUMO gap, and a blue shift in C–H (edges) out-of-plane-bending frequencies at the fingerprint region (see Supp-Figure 1, Supporting Information) for the zigzag isomer.

**4.3. Stability and Site Selectivity in  $C_{54}$  GNFs.** In the largest series, recently, the zigzag- $C_{54}H_{18}$  isomer (circumcoronene) also has been extensively studied.<sup>49,51,57,58</sup> Hence, we have considered its structural isomers with fully armchair and arm-zig edges for  $C_{54}$  GNFs along with circumcoronene for better structure–property correlation. Structural isomers of  $C_{54}$  GNFs with armchair, arm-zig, and zigzag edges are shown in Table 3. There are eight armchair pouches in the  $C_{54}H_{22}$

armchair isomer (indicated by “ac” in Table 2), and the arm-zig-C<sub>54</sub>H<sub>20</sub> isomer has four armchair pouches (indicated by “ac” in Table 3). Structure, HOMO–LUMO gap, and dispersion energies for armchair, arm-zig, and zigzag isomers are tabulated in Table 3. The HOMO–LUMO gaps for armchair, arm-zig, and zigzag isomers are 1.99, 0.02, and 1.90 eV, respectively. Also, in this series, every atom contributes to frontier molecular orbitals (see Supp-Table 1, Supporting Information). Contribution of dispersion energy toward the total energy is largest in zigzag ( $-31.40 \text{ kcal mol}^{-1}$ ) followed by that in arm-zig ( $-30.48 \text{ kcal mol}^{-1}$ ) and armchair ( $-29.65 \text{ kcal mol}^{-1}$ ). Similar to the rest of the series, also, in this series of isomers, a highest dispersion energy contribution, a high HOMO–LUMO gap, and a blue shift in C–H (edges) out-of-plane-bending frequencies at the fingerprint region (see Supp-Figure 1, Supporting Information) for the zigzag isomer indicate that zigzag-terminated GNFs are chemically less reactive (more stable) as compared to the rest of the C<sub>54</sub> isomers. Site selectivity for these isomers is discussed in the following subsections.

**4.3.1. Armchair-C<sub>54</sub>H<sub>22</sub>.** This isomer has 11 chemically distinct sites, namely, A–K (see Table 3). Among them, site D has the highest  $f_k^{\text{el}}$  (1.212) and the lowest  $f_k^{\text{nuc}}$  (0.825); hence, this site is most prone to attack by a nucleophile. Site B has the highest  $f_k^{\text{nuc}}$  (1.149) and the lowest  $f_k^{\text{el}}$  (0.870); therefore, it is most susceptible to an attack by an electrophile. The presence of a spacer atom (site E) in between sites D and B makes it an attractive candidate for hydrogenation/dehydrogenation reactions. In addition, the peripheral sites such as G, H, J, and K are amphiphilic and hence are prone to attack by both donor–acceptor functional groups with equal probability. In the rest of the sites, sites E and I are more prone to nucleophilic attack than sites A, C, and F (see Table 3). This structure does not provide any strong alternating Lewis acid–base pairs, and all interior atoms are more nucleophilic; hence, this isomer may be a potential candidate for surface functionalization by suitable electrophiles.

**4.3.2. Arm-Zig-C<sub>54</sub>H<sub>20</sub>.** In this isomer, there are 13 chemically distinct sites, namely, A–M (see Table 3). Among these sites, site A has the highest relative electrophilicity index of 1.105 and the least value for relative nucleophilicity of 0.905; hence, this site is most prone to attack by a nucleophile. Site G has the highest relative nucleophilicity index of 1.300 and the least relative electrophilicity of 0.771; therefore, it is most susceptible to attack by an electrophile. However, sites F, H, and I are amphiphilic sites with  $f_k^{\text{el}} \sim f_k^{\text{nuc}}$ . Sites B, C, D, E, and M have higher relative electrophilicity compared to sites I, K, and L and hence are prone to attack by nucleophiles. In short, the interior atoms are very reactive, and the molecule as a whole is reactive with few amphiphilic sites scattered. This is in close agreement with the reactivity of arm-zig isomers of C<sub>24</sub> and C<sub>42</sub> as projected by Fukui functions as well as from the lowest dispersion energy, lowest HOMO–LUMO gap, and a red shift in C–H (edges) out-of-plane-bending frequencies at the fingerprint region (see Supp-Figure 1, Supporting Information) with respect to the zigzag isomer. This structure does not provide any alternating Lewis acid–base pairs through out the cluster but is an interesting quantum dot for doping interior carbon atoms.

**4.3.3. Zigzag-C<sub>54</sub>H<sub>18</sub>.** This nanodisc isomer is an extension of both zigzag-C<sub>24</sub> and armchair-C<sub>42</sub> with six chemically distinct sites, namely, A–F (see Table 3). Among the six sites, site B has the highest relative electrophilicity index of 1.151 and the least

value for relative nucleophilicity of 0.869. Hence, this site is highly prone to attack by nucleophiles. Site A has the highest relative nucleophilicity index of 1.017 and the least relative electrophilicity index of 0.983. Hence, A is the most susceptible site for attack by electrophiles. Site C is the amphiphilic one, and the rest of the sites D, E, and F have  $f_k^{\text{el}} \sim f_k^{\text{nuc}}$ . Hence, the zigzag isomer may be an attractive GNF for surface functionalization importantly by nucleophiles. In this isomer, edges are the least reactive as compared to the interior carbon atoms. Interestingly, also in this case, lesser chemical reactivity (more stability) of this nanodisc isomer (circumcoronene) as projected by Fukui functions goes hand in hand with highest dispersion energy contribution, a high HOMO–LUMO gap, and a blue shift in C–H (edges) out-of-plane-bending frequencies at the fingerprint region (see Supp-Figure 1, Supporting Information) for the zigzag isomer.

**4.4. Validation of Site Selectivity by Reactivity Descriptors: A Case Study of OH<sup>−</sup>, NH<sub>2</sub><sup>−</sup>, and H<sub>2</sub>O Adsorption on Armchair-C<sub>24</sub> and Zigzag-C<sub>24</sub> GNFs.** Site selectivity projected by relative reactivity descriptors is validated on armchair-C<sub>24</sub> and zigzag-C<sub>24</sub> GNFs. We have used OH<sup>−</sup> (hydroxyl), NH<sub>2</sub><sup>−</sup> (amine), and H<sub>2</sub>O as probe molecules. The hydroxyl group is used as a probe molecule, as it is used extensively in covalent chemical functionalization. In fact, it is a very effective way of tuning the electronic properties by opening up the band gap in graphene.<sup>11–14</sup> On the other hand, amine groups react readily with graphene and are extensively used in covalent functionalization of graphene oxide.<sup>83,84</sup> Sufficient reports are available to understand the interaction of water and carbon surfaces for biological applications; hence, we have also used the water molecule as a probe for validation.

The optimized geometries and interaction energies for these GNF–nucleophile complexes are tabulated in Table 4. As discussed earlier in Section 4.1.1, the most probable sites for nucleophilic and electrophilic attacks on armchair-C<sub>24</sub> are sites F and E, respectively. When a hydroxyl group adsorbs on site F, it forms a strong chemical bond with an interaction energy of 52.48 kcal mol<sup>−1</sup> while on site E its interaction energy is 42.71 kcal mol<sup>−1</sup>. Next, when an amine group adsorbs on sites F and E, the interaction energies are 59.12 and 51.70 kcal mol<sup>−1</sup>, respectively. A higher interaction energy of hydroxyl and amine groups with site F thus validates the trends predicted by reactivity descriptors. In both cases, bonded carbon atoms project out of the plane of the GNF (see Table 4) leading to a change of hybridization from sp<sup>2</sup> to sp<sup>3</sup>. Finally, we have also carried out an explicit water molecule adsorption on both sites. The difference in the interaction energies (see Table 4) is quite small for this case as compared to the hydroxyl and amine groups, suggesting van der Waals interaction between the water molecule and the GNF. Nevertheless, its force of attraction is more on site F than on site E validating the site selectivity in armchair-C<sub>24</sub>.

A similar trend is observed while validating the site selectivity in hydrogen-terminated zigzag-C<sub>24</sub> GNF. The optimized geometries and interaction energies are as shown in Table 4. As mentioned in Section 4.1.3, the most favorable site for nucleophilic attack on zigzag-C<sub>24</sub> are sites B and C as they are amphiphilic. Since, the only other site, namely, site A is more favorable for electrophilic attack, we have chosen sites A and B for validation purpose. Adsorption of a hydroxyl group yields interaction energies of 43.16 and 45.86 kcal mol<sup>−1</sup> on sites A and B, respectively. Similarly, the amine group on sites A and B has interaction energies of 53.53 and 54.66 kcal mol<sup>−1</sup>,

respectively. Similar to armchair-C<sub>24</sub> GNF, there is a change of hybridization from sp<sup>2</sup> to sp<sup>3</sup> in the zigzag-C<sub>24</sub> isomer as well. Water molecule adsorption on these sites yields also a similar result as seen in armchair-C<sub>24</sub>. However, the most interesting point to note is that the differences in adsorption energies between the two sites for the hydroxyl and the amine group in this GNF is much lower as compared to the adsorption energy differences on the two sites of armchair-C<sub>24</sub>. This is consistent with the fact that the nucleophilic sites of armchair-C<sub>24</sub> are stronger (the indices are higher) as compared to the nucleophilic sites of the zigzag-C<sub>24</sub> GNF.

## 5. CONCLUSIONS

In this study, we have made an attempt to discern the site selectivity in small-sized GNFs using spin-polarized and dispersion-corrected DFT. Findings reveal that, among the armchair, arm-zig, and zigzag isomers of C<sub>24</sub>, C<sub>42</sub>, and C<sub>54</sub> GNFs, (i) zigzag isomers have the largest dispersion energy contribution toward the total energy of the system and a high HOMO–LUMO energy gap; (ii) a blue shift in the C–H (edges) out-of-plane-bending frequencies at the fingerprint region suggests the lesser chemical reactivity of zigzag-terminated GNFs, which are in close agreement with the reactivity trends projected by Fukui functions; (iii) in contrast, arm-zig isomers are chemically very reactive as compared to armchair and zigzag isomers by possessing lower dispersion energy, the lowest HOMO–LUMO energy gap, and a red shift in the C–H (edges) out-of-plane-bending frequencies at the fingerprint region; (iv) chemical reactivity of all armchair isomers lie in between zigzag and arm-zig isomers; and (iv) on the basis of these observations, it is concluded that the order of stability is zigzag > armchair > arm-zig, and the order of reactivity is contrary.

Thus, we observe a critical dependence of reactivity on shape, size, and type of edges. These trends along with the directionality of the frontier molecular orbitals can be effectively used for controlled redox reactions on system specific GNFs. Thus, isomers can be chosen for chemical functionalization with chemo/regioselective donor–acceptor functional groups at the interior as well as at peripheral sites. In short, a strong discernment on site selectivity and the synthesis of definite edge geometry offer promising solutions to molecular- and nanoelectronics.

## ■ ASSOCIATED CONTENT

### S Supporting Information

Frontier molecular orbitals of GNFs and vibrational frequencies for edges of all GNF isomers. This material is available free of charge via the Internet at <http://pubs.acs.org>.

## ■ AUTHOR INFORMATION

### Corresponding Author

\*E-mail: sailaja.raaj@gmail.com.

### Notes

The authors declare no competing financial interest.

## ■ ACKNOWLEDGMENTS

M.A.N. acknowledges the Department of Science and Technology (DST), New Delhi for funding through a JRF-INSPIRE fellowship. The authors acknowledge the Center of Excellence in Scientific Computing (COESC) at CSIR-National Chemical Laboratory (NCL), Pune, for the

calculations presented here. The authors also acknowledge the CSIR-Central Electro Chemical Research Institute (CECRI), Karaikudi, and the CSIR-Fourth Paradigm Institute (4PI) for providing high-performance computing facilities. S.K. acknowledges the CSIR 12<sup>th</sup> five year plan MSM project (CSC-0129) grant. S.K. and K.L.N.P. acknowledge a grant from the Indo-Australian project (CLP-10/11). M.A.N. acknowledges Dr. K. Selvaraj, CSIR-NCL, for his valuable suggestions. Authors also acknowledge the suggestions given by the reviewers.

## ■ REFERENCES

- (1) Novoselov, K. S.; Geim, A. K.; Morozov, S. V.; Jiang, D.; Zhang, Y.; Dubonos, S. V.; Grigorieva, I. V.; Firsov, A. A. Electric Field Effect in Atomically Thin Carbon Films. *Science* **2004**, *306*, 666–669.
- (2) Novoselov, K. S.; Geim, A. K.; Morozov, S. V.; Jiang, D.; Katsnelson, M. I.; Grigorieva, I. V.; Dubonos, S. V.; Firsov, A. A. Two-Dimensional Gas Of Massless Dirac Fermions in Graphene. *Nature* **2005**, *438*, 197–200.
- (3) Novoselov, K. S.; Jiang, Z.; Zhang, Y.; Morozov, S. V.; Stromer, H. L.; Zeitler, U.; Maan, J. C.; Boebinger, G. S.; Kim, P.; Geim, A. K. Room-Temperature Quantum Hall Effect in Graphene. *Science* **2007**, *315*, 1359.
- (4) Beenakker, C. W. J. Andreev Reflection and Klein Tunneling in Graphene. *Rev. Mod. Phys.* **2008**, *80*, 1337–1354.
- (5) Du, X.; Skachko, I.; Barker, A.; Andrei, E. Y. Approaching Ballistic Transport in Suspended Graphene. *Nat. Nanotechnol.* **2008**, *3*, 491.
- (6) Balandin, A. A.; Ghosh, S.; Bao, W. Z.; Calizo, I.; Teweldebrhan, D.; Miao, F.; Lau, C. N. Superior Thermal Conductivity of Single-Layer Graphene. *Nano Lett.* **2008**, *8*, 902.
- (7) Nair, R. R.; Blake, P.; Grigorenko, A. N.; Novoselov, K. S.; Booth, T. J.; Stauber, T.; Peres, N. M. R.; Geim, A. K. Fine Structure Constant Defines Visual Transparency of Graphene. *Science* **2008**, *320*, 1308.
- (8) Latil, S.; Henrard, L. Charge Carriers in Few-Layer Graphene Films. *Phys. Rev. Lett.* **2006**, *97*, 036803.
- (9) Castro Neto, A.; Guinea, F.; Peres, N. M. R.; Novoselov, K.; Geim, A. The Electronic Properties of Graphene. *Rev. Mod. Phys.* **2009**, *81*, 109.
- (10) Abergel, D.; Apalkov, V.; Berashevich, J.; Zieler, K.; Chakraborty, T. Properties of Graphene: A Theoretical Perspective. *Adv. Phys.* **2010**, *59*, 261.
- (11) Yan, J.-A.; Xian, L.; Chou, M. Y. Structural and Electronic Properties of Oxidized Graphene. *Phys. Rev. Lett.* **2009**, *103* (086802), 14.
- (12) Yan, J.-A.; Chou, M. Y. Oxidation Functional Groups on Graphene: Structural and Electronic Properties. *Phys. Rev. Lett.* **2010**, *82* (125403), 110.
- (13) Park, S.; Ruoff, R. Chemical Methods for the Production of Graphenes. *Nat. Nano.* **2009**, *4*, 217–224.
- (14) Akbar Bagri, A.; Mattevi, C.; Acik, M.; Chabal, Y. J.; Chhowalla, M.; Shenoy, V. B. Structural Evolution during the Reduction of Chemically Derived Graphene Oxide. *Nat. Chem.* **2010**, *2*, 581587.
- (15) Sessi, P.; Guest, J. R.; Bode, M.; Guisinger, N. P. Patterning Graphene at the Nanometer Scale via Hydrogen Desorption. *Nano Lett.* **2009**, *9*, 4343–4347.
- (16) Haberer, D.; Vyalikh, D. V.; Taioli, S.; Dora, B.; Farjam, M.; Fink, J.; Marchenko, D.; Pichler, T.; Ziegler, K.; Simonucci, S.; et al. Tunable Band Gap in Hydrogenated Quasi-Free-Standing Graphene. *Nano Lett.* **2010**, *10*, 3360–3366.
- (17) Yang, M.; Nurbawono, A.; Zhang, C.; Feng, Y. P.; Ariando. Two-Dimensional Graphene Superlattice Made with Partial Hydrogenation. *Appl. Phys. Lett.* **2010**, *96*, 193115.
- (18) Zhou, J.; Wang, Q.; Chen, X. S.; Kawazoe, Y.; Jena, P. Ferromagnetism in Semihydrogenated Graphene Sheet. *Nano Lett.* **2009**, *9*, 3867–3870.
- (19) Son, Y.; Cohen, M.; Louie, S. Half-Metallic Graphene Nanoribbon. *Nature* **2006**, *444*, 347.

- (20) Son, Y.; Cohen, M.; Louie, S. Energy Gaps in Graphene Nanoribbons. *Phys. Rev. Lett.* **2006**, *97*, 216803.
- (21) Sakai, K.; Takai, K.; Fukui, K.; Nakanishi, T.; Enoki, T. Honeycomb Super Periodic Pattern and Its Fine Structure Near the Armchair Edge of Graphene Observed by Low-Temperature Scanning Tunneling Microscopy. *Phys. Rev. B* **2010**, *81*, 235417.
- (22) Sasaki, K.; Wakabayashi, K.; Enoki, T. Berry's Phase for Standing Waves near Graphene Edge. *New J. Phys.* **2010**, *12*, 083023.
- (23) Fujita, M.; Wakabayashi, K.; Nakada, K.; Kusakabe, K. Peculiar Localized State at Zigzag Graphite Edge. *J. Phys. Soc. Jpn.* **1996**, *65*, 1920–1923.
- (24) Nakada, K.; Fujita, M.; Dresselhaus, G.; Dresselhaus, M. S. Edge State in Graphene Ribbons: Nanometer Size Effect and Edge Shape Dependence. *Phys. Rev. B* **1996**, *54*, 17954–17961.
- (25) Kobayashi, Y.; Fukui, K.; Enoki, T.; Kusakabe, K.; Kaburagi, Y. Observation of Zigzag and Armchair Edges of Graphite Using Scanning Tunneling Microscopy and Spectroscopy. *Phys. Rev. B* **2005**, *71*, 193406.
- (26) Barnard, A. S.; Snook, I. K. Modelling the Role of Size, Edge Structure and Terminations on the Electronic Properties of Graphene Nano-Flakes. *Modell. Simul. Mater. Sci. Eng.* **2011**, *19*, 054001.
- (27) Shi, H.; Barnard, A. S.; Snook, I. K. Modelling the Role of Size, Edge Structure and Terminations on the Electronic Properties of Trigonal Graphene Nanoflakes. *Nanotechnology* **2012**, *23*, 065707.
- (28) Fujii, S.; Enoki, T. Nanographene and Graphene Edges: Electronic Structure and Nanofabrication. *Acc. Chem. Res.* **2013**, *46* (10), 2201–2210.
- (29) Yang, Y.; Raghunath, M. Impact of Size Effect on Graphene Nanoribbon Transport. *IEEE Electron Device Lett.* **2010**, *31* (3), 237–239.
- (30) Betti, A.; Fiori, G.; Iannaccone, G. Strong Mobility Degradation in Ideal Graphene Nanoribbons due to Phonon Scattering. *Appl. Phys. Lett.* **2011**, *98*, 212111.
- (31) Rader, H.; Rouhani, A.; Talarico, A.; Palermo, V.; Samori, P.; Mullen, K. Processing of Giant Graphene Molecules by Soft-Landing Mass Spectroscopy. *Nat. Mater.* **2006**, *5*, 276–280.
- (32) Wu, X.; Zeng, X. Sawtooth-like Graphene Nanoribbons. *Nano Res.* **2008**, *1*, 40–45.
- (33) Zhi, L.; Mullens, K. A Bottom-Up Approach from Molecular Nanographenes to Unconventional Materials. *J. Mater. Chem.* **2008**, *18*, 1472–1484.
- (34) Park, S.; Ruoff, R. Chemical Methods for the Production of Graphenes. *Nat. Nanotechnol.* **2009**, *4*, 217–224.
- (35) Terrones, M. Nanotubes Unzipped. *Nature* **2009**, *458*, 845–846.
- (36) Snook, I. K.; Barnard, A. S. Graphene Nano-Flakes and Nano-Dots: Theory, Experiment and Applications. In *Physics and Applications of Graphene - Theory*; Mikhailov, S., Ed.; InTech: Rijeka, Croatia, 2011.
- (37) Shang, N. G.; Papakonstantinou, P.; McMullan, M.; Chu, M.; Stamboulis, A.; Potenza, A.; Dhesi, S. S.; Marchetto, H. Catalyst-Free Efficient Growth, Orientation and Biosensing Properties of Multilayer Graphene Nanoflake Films with Sharp Edge Planes. *Adv. Funct. Mater.* **2008**, *18*, 3506–3514.
- (38) Vadukumpally, S.; Paul, J.; Valiyaveettill, S. Cationic Surfactant Mediated Exfoliation of Graphite into Graphene Flakes. *Carbon* **2009**, *47*, 3288–3294.
- (39) Vadukumpally, S.; Paul, J.; Mahanta, N.; Valiyaveettill, S. Flexible Conductive Graphene/Poly(Vinyl Chloride) Composite Thin Films with High Mechanical Strength and Thermal Stability. *Carbon* **2011**, *49*, 198–205.
- (40) Vadukumpally, S.; Gupta, J.; Zhang, Y. P.; Xu, G. Q.; Valiyaveettill, S. Functionalization of Surfactant Wrapped Graphene Nanosheets with Alkylazides for Enhanced Dispersability. *Nanoscale* **2011**, *3*, 303–308.
- (41) Barnard, A. S.; Snook, I. K. Transformation of Graphene into Graphane in the Absence of Hydrogen. *Carbon* **2010**, *48*, 981.
- (42) Barnard, A. S.; Snook, I. K. Size and Shape-Dependence of the Graphene to Graphane Transformation in the Absence of Hydrogen. *J. Mater. Chem.* **2010**, *20*, 10459.
- (43) Kuc, A.; Heine, T.; Seifert, G. Structural and Electronic Properties of Graphene Nanoflakes. *Phys. Rev. B* **2010**, *81*, 085430.
- (44) Hongqing, S.; Barnard, A. S.; Snook, I. K. Quantum Mechanical Properties of Graphene Nano-Flakes and Quantum Dots. *Nanoscale* **2012**, *4*, 6761.
- (45) Singh, S. K.; Neek-Amal, M.; Peeters, F. M. Electronic Properties of Graphene Nano-Flakes: Energy Gap, Permanent Dipole, Termination Effect, and Raman Spectroscopy. *J. Chem. Phys.* **2012**, *140* (7), 074304.
- (46) Umadevi, D.; Sastry, G. N. Molecular and Ionic Interaction with Graphene Nanoflakes: A Computational Investigation of CO<sub>2</sub>, H<sub>2</sub>O, Li, Mg, Li<sup>+</sup>, and Mg<sup>2+</sup> Interaction with Polycyclic Aromatic Hydrocarbons. *J. Phys. Chem. C* **2011**, *115*, 9656–9667.
- (47) Barnard, A. S.; Snook, I. K. Ideality versus Reality: Predicting the Effect of Realistic Environments on the Electronic Properties of Nanographene. *Nanosci. Nanotechnol. Lett.* **2011**, *3*, 59.
- (48) Shi, H.; Lai, L.; Snook, I. K.; Barnard, A. S. Relative Stability of Graphene Nanoflakes under Environmentally Relevant Conditions. *J. Phys. Chem. C* **2013**, *117*, 15375–15382.
- (49) Haldar, S.; Kolar, M.; Sedla, R. K.; Hobza, P. Adsorption of Organic Electron Acceptors on Graphene-like Molecules: Quantum Chemical and Molecular Mechanical Study. *J. Phys. Chem. C* **2012**, *116*, 25328–25336.
- (50) Yavari, F.; Koratkar, N. Graphene-Based Chemical Sensors. *J. Phys. Chem. Lett.* **2012**, *3*, 1746–1753.
- (51) Schyman, P.; Jorgensen, W. L. Exploring Adsorption of Water and Ions on Carbon Surfaces Using a Polarizable Force Field. *J. Phys. Chem. Lett.* **2013**, *4*, 468–474.
- (52) Balamurugan, K.; Subramanian, V. Adsorption of Chlorobenzene onto (S,S) Armchair Single-Walled Carbon Nanotube and Graphene Sheet: Toxicity versus Adsorption Strength. *J. Phys. Chem. C* **2013**, *117* (41), 21217–21227.
- (53) Fan, X.; Zheng, W. T.; Kuo, J.-L. Adsorption and Diffusion of Li on Pristine and Defective Graphene. *ACS Appl. Mater. Interfaces* **2012**, *4* (S), 2432–2438.
- (54) Patra, N.; Esan, D. A.; Krl, P. Dynamics of Ion Binding to Graphene Nanostructures. *J. Phys. Chem. C* **2013**, *117* (20), 10750–10754.
- (55) Lu, C. H.; Yang, H. H.; Zhu, C. L.; Chen, X.; Chen, G. N. A Graphene Platform for Sensing Biomolecules. *Angew. Chem., Int. Ed.* **2009**, *48*, 4785–4787.
- (56) Shan, C. S.; Yang, H. F.; Song, J. F.; Han, D. X.; Ivaska, A.; Niu, L. Direct Electrochemistry of Glucose Oxidase and Biosensing for Glucose Based on Graphene. *Anal. Chem.* **2009**, *81*, 2378–2382.
- (57) Silva, A. M.; Pires, M. S.; Freire, V. N.; Albuquerque, E. L.; Azevedo, D. L.; Caetano, E. W. S. Graphene Nanoflakes: Thermal Stability, Infrared Signatures, and Potential Applications in the Field of Spintronics and Optical Nanodevices. *J. Phys. Chem. C* **2010**, *114*, 17472–17485.
- (58) Barnard, A. S.; Snook, I. K. Thermal Stability of Graphene Edge Structure and Graphene Nanoflakes. *J. Chem. Phys.* **2008**, *128*, 094707.
- (59) Pietrucci, F.; Andreoni, W. Fate of a Graphene Flake: A New Route Toward Fullerenes Disclosed with ab Initio Simulations. *J. Chem. Theory Comput.* **2014**, *10* (3), 913–917.
- (60) Cao, Y.; Osuna, S.; Liang, Y.; Haddon, R. C.; Houk, K. N. Diels–Alder Reactions of Graphene: Computational Predictions of Products and Sites of Reaction. *J. Am. Chem. Soc.* **2013**, *135*, 17643–17649.
- (61) Denis, P. A. Organic Chemistry of Graphene: The Diels–Alder Reaction. *Chem.—Eur. J.* **2013**, *19*, 15719–15725.
- (62) Hohenberg, P.; Kohn, W. Inhomogeneous Electron Gas. *Phys. Rev.* **1964**, *136*, B864–B871.
- (63) Parr, R. G.; Yang, W. Density Functional Approach to the Frontier-Electron Theory of Chemical Reactivity. *J. Am. Chem. Soc.* **1984**, *106*, 4049–4051.

- (64) Fukui, K.; Yonezawa, T.; Shingu, H. A Molecular Orbital Theory of Reactivity in Aromatic Hydrocarbons. *J. Chem. Phys.* **1952**, *20*, 722.
- (65) Fukui, K. *Theory of Orientation and Stereoselection*; Springer: New York, 1973.
- (66) Fukui, K. Role of Frontier Orbitals in Chemical Reactions. *Science* **1982**, *218*, 747.
- (67) Perdew, J. P.; Parr, R. G.; Levy, M.; Balduz, J. L., Jr. Density Functional Theory for Fractional Particle Number: Derivative Discontinuities of the Energy. *Phys. Rev. Lett.* **1982**, *49*, 1691–1695.
- (68) Zhang, Y.; Yang, W. Perspective on “Density Functional Theory for Fractional Particle Number: Derivative Discontinuities of the Energy”. *Theor. Chem. Acc.* **2000**, *103*, 346–348.
- (69) De Proft, F.; Amira, S.; Choho, K.; Geerlings, P. Quantum-Chemical Study of the Acidity of Substituted Acetic Acids with Density Functional Theory Based Descriptors. *J. Phys. Chem.* **1994**, *98*, 5227–5233.
- (70) Yang, W.; Mortier, W. The Use of Global and Local Molecular Parameters for the Analysis of the Gas-Phase Basicity of Amines. *J. Am. Chem. Soc.* **1986**, *108*, 5708–5711.
- (71) Roy, R. K.; Krishnamurti, S.; Geerlings, P.; Pal, S. Local Softness and Hardness Based Reactivity Descriptors for Predicting Intra- and Intermolecular Reactivity Sequences: Carbonyl Compounds. *J. Phys. Chem. A* **1998**, *102*, 3746–3755.
- (72) Roy, R. K.; de Proft, F. de.; Geerlings, P. Site of Protonation in Aniline and Substituted Anilines in the Gas Phase: A Study via the Local Hard and Soft Acids and Bases Concept. *J. Phys. Chem. A* **1998**, *102*, 7035–7040.
- (73) Faver, J.; Merz, K. M., Jr. Utility of the Hard/Soft Acid-Base Principle via the Fukui Function in Biological Systems. *J. Chem. Theory Comput.* **2010**, *6*, 548–559.
- (74) De, H. S.; Krishnamurti, S.; Pal, S. Understanding the Reactivity Properties of Au<sub>n</sub> ( $6 \leq n \leq 13$ ) Clusters Using Density Functional Theory Based Reactivity Descriptors. *J. Phys. Chem. C* **2010**, *114*, 6690–6703.
- (75) Allison, T. C.; Tong, Y. J. Applications of the Condensed Fukui Function to Predict Reactivity in Core-Shell Transition Metal Nanoparticles. *Electrochim. Acta* **2013**, *101*, 334–340.
- (76) Kohn, W.; Sham, L. J. Quantum Density Oscillations in an Inhomogeneous Electron Gas. *Phys. Rev.* **1965**, *137*, A1697–A1705.
- (77) Kohn, W.; Sham, L. J. Self-Consistent Equations Including Exchange and Correlation Effects. *Phys. Rev.* **1965**, *140*, A1133–A1138.
- (78) Koster, A. M.; Calaminici, P.; Casida, M. E.; Moreno, R. F.; Geudtner, G.; Goursot, A.; Heine, T.; Ipatov, A.; Janetzko, F.; del Campo, J. M.; Patchkovskii, S.; Reveles, J. U.; Vela, A.; Salahub, D. R. *deMon2.2.6*; 2006.
- (79) Goursot, A.; Mineva, T.; Kevorkyants, R.; Talbi, D. Interaction between *n*-Alkane Chains: Applicability of the Empirically Corrected Density Functional Theory for Van der Waals Complexes. *J. Chem. Theory Comput.* **2007**, *3*, 755.
- (80) Perdew, J. P.; Burke, K.; Ernzerhof, M. Generalized Gradient Approximation Made Simple. *Phys. Rev. Lett.* **1996**, *77*, 3865.
- (81) Godbout, N.; Salahub, D. R.; Wimmer, J. A. E. Optimization of Gaussian-Type Basis Sets for Local Spin Density Functional Calculations. Part I. Boron through Neon, Optimization Technique and Validation. *Can. J. Phys.* **1992**, *70*, 560.
- (82) Löwdin, P. O. On the Nonorthogonality Problem Connected with the Use of Atomic Wave Functions in the Theory of Molecules and Crystals. *J. Chem. Phys.* **1950**, *18*, 365.
- (83) Lomeda, J. R.; Doyle, C. D.; Kosynkin, D. V.; Hwang, W.-F.; Tour, J. M. Diazonium Functionalization of Surfactant-Wrapped Chemically Converted Graphene Sheets. *J. Am. Chem. Soc.* **2008**, *130*, 16201–16206.
- (84) Milowska, K. Z.; Majewski, J. A. Stability and Electronic Structure of Covalently Functionalized Graphene Layers. *Phys. Status Solidi B* **2013**, *250* (8), 1474–1477.